

# Distribution of light at and near the focus of high-numerical-aperture objectives

M. Mansuripur

College of Engineering, Boston University, 110 Cummington Street, Boston, Massachusetts 02215

Received December 20, 1985; accepted July 23, 1986

Classical diffraction theory is used to investigate the effects of high numerical aperture on the focusing of coherent light. By expanding the diffracted beam in plane waves, we show that the lens action can be expressed as a succession of three Fourier transforms. Furthermore, polarization effects are included in the model in a natural way. Some numerical results of the theory are also presented.

## 1. INTRODUCTION

To achieve high resolution in many optical systems of practical interest, it is necessary to use high-numerical-aperture objectives. For instance, in optical data storage one must focus the laser beam to extremely small spots for recording and readout of information. For a well-corrected lens, the limit of resolution is the radius of the Airy disk, which is equal to  $0.61\lambda/\text{NA}$ . Here  $\lambda$  is the wavelength of light and  $\text{NA} = \sin(\alpha/2)$  is the numerical aperture, with  $\alpha$  being the angle subtended by the exit pupil at the focal point. Standard approximations of the classical diffraction theory can be used to describe the field pattern around the focal plane, but, strictly speaking, these approximations are valid only for  $\text{NA} \lesssim \sqrt[4]{\lambda/f}$ . When the focal length is  $f = 4000\lambda$ , for example, the upper limit of validity of the standard approximations is  $\text{NA} = 0.125$ .

Hopkins<sup>1</sup> has shown that a more rigorous treatment yields almost the same results as the approximate method, provided that the aperture radius is taken to be  $f\text{NA}$  [as opposed to  $f \tan[\arcsin(\text{NA})]$ ]. The Hopkins method, however, is relatively complicated, and some of its assumptions are open to question. Moreover, it is not easy to generalize his treatment to situations in which the incident distribution is non-uniform. Other authors have studied the focusing problem in various regimes with different approximations, but, to our knowledge, there does not exist a comprehensive method of computing diffraction patterns that does not require approximations of one sort or another to the fundamental diffraction integral. To be sure, the fundamental integral of the classical theory is itself an approximation to the physical reality since it does not include the effect of the screen on the aperture field distribution. This approximation, however, turns out to be quite acceptable as long as the dimensions of interest are not comparable to or smaller than a wavelength.

In this paper we present a formulation of the Fresnel-Kirchhoff diffraction theory that allows polarization effects to be incorporated in a natural way. We show that the diffraction integral can be exactly evaluated in the near-field regime with two successive Fourier transforms; in the far-field regime, where the exact computations become impractical, the steepest-descent approximation applies to the integral, yielding the Fraunhofer formula that requires only

one Fourier transform. Next we consider diffraction in the presence of a lens and show that for small numerical apertures, where the curvatures introduced by the lens are slight, the propagation formulas of Fresnel or Fraunhofer are still applicable. For large numerical apertures, however, these methods become excessively time consuming; in this regime, we factor out the fast-oscillating terms of the curvature function and obtain a practical formula for computing diffraction patterns using three successive Fourier transformations.

The organization of this paper is as follows: Section 2 describes the formulation of diffraction theory, including polarization, using plane-wave expansion of the incident distribution. Sections 3 and 4 are devoted to propagation in the far-field and near-field regimes, respectively. In Section 5 the effect of focusing on the distribution around the focal plane is discussed; also, some of the results are compared with the experimental or theoretical works of other authors. Results of numerical computations are presented in Section 6.

## 2. THEORY OF DIFFRACTION

In this section we introduce the framework for the analyses presented in the rest of the paper. Our approach to diffraction theory is only slightly different from the classical approach based on the Fresnel-Kirchhoff formulation,<sup>2</sup> and the results can be shown to be identical with those of the classical theory. The advantages of the adopted approach are that the range of validity of various approximations is easily identified and that extensions to situations in which these approximations are no longer applicable become straightforward; moreover, polarization effects can be included in the theory in a natural way. The approach is based on the plane-wave expansion of the incident distribution and the eventual recombination of the propagated waves.

Consider a plane, monochromatic wave of wavelength  $\lambda$ , traveling in the direction of the unit vector  $\hat{\sigma} = (\sigma_x, \sigma_y, \sigma_z)$ . The space-time dependence of this wave is given by

$$A(x, y, z, t) = A_0 \exp[i(2\pi/\lambda)(x\sigma_x + y\sigma_y + z\sigma_z)] \exp[-i\omega t]. \quad (1)$$

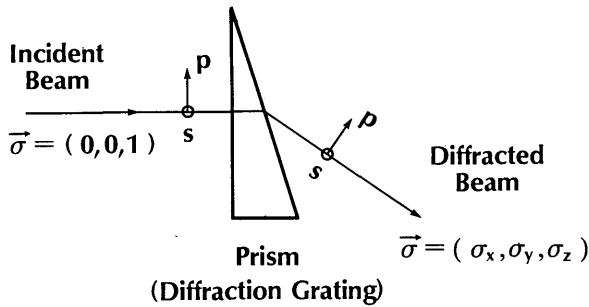


Fig. 1. Prism as a diffraction grating: A plane, linearly polarized incident beam is diffracted into a plane wave propagating in the direction  $\hat{\sigma} = (\sigma_x, \sigma_y, \sigma_z)$ . The polarization of the outgoing beam is related to the polarization of the incoming beam and the orientation of the prism as described in the text.

The polarization is in the plane perpendicular to  $\hat{\sigma}$  but is otherwise arbitrary. Ignoring the time dependence for the time being and confining our attention to the plane  $Z = 0$ , we find that the amplitude distribution is given by

$$A(x, y) = A_0 \exp[i(2\pi/\lambda)(x\sigma_x + y\sigma_y)], \quad (2)$$

where  $\sigma_x^2 + \sigma_y^2 \leq 1$ .

Now, assuming an arbitrary distribution  $t(x, y)$  in the plane  $Z = 0$ , define the Fourier transform of  $t(x, y)$  as

$$T(S_x, S_y) = \iint_{-\infty}^{+\infty} t(x, y) \exp[-i2\pi(xS_x + yS_y)] dx dy. \quad (3)$$

The inverse Fourier-transform relation then yields

$$t(x, y) = \lambda^{-2} \iint_{-\infty}^{+\infty} T(\sigma_x/\lambda, \sigma_y/\lambda) \times \exp[i(2\pi/\lambda)(x\sigma_x + y\sigma_y)] d\sigma_x d\sigma_y. \quad (4)$$

Comparing Eqs. (2) and (4), one concludes that  $t(x, y)$  is the superposition of plane waves propagating in various directions. The amplitudes of these plane waves are determined by the Fourier transform of  $t(x, y)$ . Of course, there is the restriction on  $(\sigma_x, \sigma_y)$  that  $\sigma_x^2 + \sigma_y^2$  must be less than unity, but the components of  $t(x, y)$  that correspond to  $(\sigma_x, \sigma_y)$  beyond the unit circle are, in fact, evanescent waves that do not carry energy and do not travel more than a few wavelengths.<sup>2</sup> Consequently, except in the immediate neighborhood of the plane  $Z = 0$ , the representation of  $t(x, y)$  as the superposition of plane waves is valid.

Turning now to the effects of polarization, let us assume that the incident beam is a linearly polarized plane wave, traveling in the  $Z$  direction, with a polarization vector along  $X$ . To determine the polarization of the diffracted beam along the vector  $\hat{\sigma} = [\sigma_x, \sigma_y, (1 - \sigma_x^2 - \sigma_y^2)^{1/2}]$ , imagine a prism (which happens to be the simplest diffraction grating) inserted between the incoming and outgoing plane waves, as shown in Fig. 1. Now consider the plane formed by the vector  $\hat{\sigma}$  and the  $Z$  axis. The component of the incident polarization vector perpendicular to this plane retains its direction and becomes the  $s$  component of the deflected beam. The projection of the incident polarization onto the above plane, however, is reoriented as the beam goes through the prism and becomes the  $p$  component of the deflected beam. These two components are given by

$$s \text{ component} = |\sigma_y|(\sigma_x^2 + \sigma_y^2)^{-1/2},$$

$$p \text{ component} = |\sigma_x|(\sigma_x^2 + \sigma_y^2)^{-1/2}.$$

When the deflected beam arrives at the plane  $Z = z_0$  it will have components of polarization along the  $X, Y$ , and  $Z$  axes. These components will be denoted  $\Psi_x, \Psi_y$ , and  $\Psi_z$  and are given by

$$\Psi_x = \frac{[\sigma_x^2 (1 - \sigma_x^2 - \sigma_y^2)^{1/2} + \sigma_y^2]}{\sigma_x^2 + \sigma_y^2}, \quad (5a)$$

$$\Psi_y = \frac{-\sigma_x \sigma_y [1 - (1 - \sigma_x^2 - \sigma_y^2)^{1/2}]}{\sigma_x^2 + \sigma_y^2}, \quad (5b)$$

$$\Psi_z = -\sigma_x, \quad (5c)$$

where it can be verified that  $\Psi_x^2 + \Psi_y^2 + \Psi_z^2 = 1$ .

Combining Eqs. (1), (4), and (5), one arrives at the following expression for the distribution of light at  $Z = z_0$ :

$$t_\alpha(x, y, z_0) = \lambda^{-2} \iint_{\sigma_x^2 + \sigma_y^2 \leq 1} \Psi_\alpha(\sigma_x, \sigma_y) T(\sigma_x/\lambda, \sigma_y/\lambda) \times \exp\{i(2\pi/\lambda)[x\sigma_x + y\sigma_y + z_0(1 - \sigma_x^2 - \sigma_y^2)^{1/2}]\} \times d\sigma_x d\sigma_y, \quad (6)$$

The subscript  $\alpha$  in Eq. (6) indicates the polarization component of the final distribution and could be  $x, y$ , or  $z$ .

Equation (6) is our basic diffraction equation and, as shown in the following sections, is equivalent to the Fresnel-Kirchhoff equation in various limits. The restriction imposed on the domain of integration in Eq. (6) results in a power-transmission coefficient  $\eta$  less than unity. This coefficient is defined by

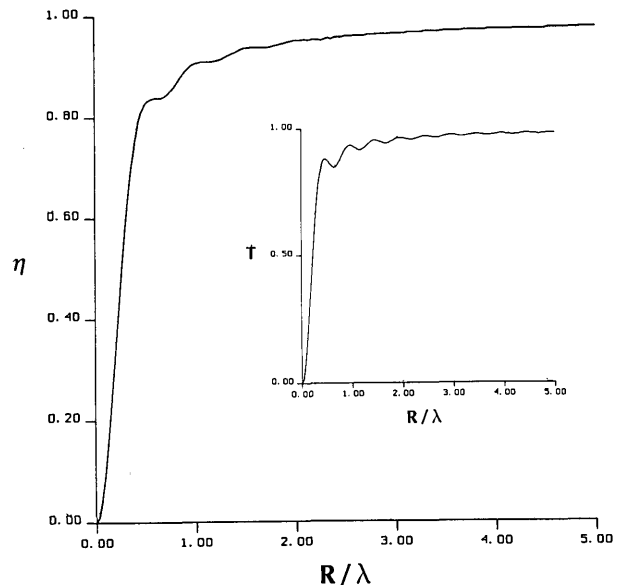


Fig. 2. Power-transmission coefficient for a circular aperture versus the normalized aperture radius. The inset shows the transmission coefficient obtained from the vector Smythe-Kirchhoff approximation according to the following equation:  $\eta = 1 - (\lambda/4\pi R) \int_0^{4\pi R/\lambda} J_0(x) dx$ .

$$\eta = \frac{\iint_{\sigma_x^2 + \sigma_y^2 \leq 1} |T(\sigma_x/\lambda, \sigma_y/\lambda)|^2 d\sigma_x d\sigma_y}{\iint_{-\infty}^{+\infty} |T(\sigma_x/\lambda, \sigma_y/\lambda)|^2 d\sigma_x d\sigma_y} \quad (7)$$

For a circular aperture of radius  $R$ , illuminated with a normally incident plane wave, the transmission coefficient calculated from Eq. (7) is

$$\eta = \int_0^1 (2/x) J_1^2(2\pi R x/\lambda) dx = 1 - J_0^2(2\pi R/\lambda) - J_1^2(2\pi R/\lambda) \quad (8)$$

$J_0$  and  $J_1$  are Bessel functions of the first kind. Figure 2 is a plot of  $\eta$  versus  $R/\lambda$ . The small-aperture limit in this figure is not expected to be correct, since in deriving Eq. (8) we have ignored the effect of the screen on the field distribution within the aperture. The inset in Fig. 2 shows the corresponding curve obtained from the vector Smythe-Kirchhoff approximation.<sup>3</sup> The two curves are in good agreement as far as general behavior is concerned. Small differences are due to the fact that the latter curve accounts for the (conducting) screen and, in part, to the approximate nature of this curve.

### 3. FRAUNHOFER OR FAR-FIELD DIFFRACTION

To derive the far-field diffraction formula from the results of the preceding section, consider the function

$$W(\sigma_x, \sigma_y) = x\sigma_x + y\sigma_y + z_0(1 - \sigma_x^2 - \sigma_y^2)^{1/2},$$

which appears in the exponent of the integrand in Eq. (6). This function has a saddle point at  $(\sigma_{x0}, \sigma_{y0})$ , where

$$\begin{aligned} \sigma_{x0} &= x/(x^2 + y^2 + z_0^2)^{1/2}, \\ \sigma_{y0} &= y/(x^2 + y^2 + z_0^2)^{1/2}. \end{aligned}$$

These are the angular coordinates of the point  $(x, y)$  in the observation plane as observed from the center of the aperture. Around this saddle point, the function  $W$  can be approximated as

$$\begin{aligned} W(\sigma_x, \sigma_y)/(x^2 + y^2 + z_0^2)^{1/2} &= 1 - 1/2[1 + (x/z_0)^2](\sigma_x - \sigma_{x0})^2 \\ &\quad - (xy/z_0^2)(\sigma_x - \sigma_{x0})(\sigma_y - \sigma_{y0}) - 1/2[1 + (y/z_0)^2](\sigma_y - \sigma_{y0})^2. \end{aligned} \quad (9)$$

Using the method of steepest descent (see Ref. 2, App. III) and replacing for the exponent of the integrand in Eq. (6) from Eq. (9), one obtains

$$\begin{aligned} t_\alpha(x, y, z_0) &= -(i/\lambda) \frac{\exp[i(2\pi/\lambda)(x^2 + y^2 + z_0^2)^{1/2}]}{z_0[1 + (x^2 + y^2)/z_0^2]} \\ &\quad \times \Psi_\alpha(\sigma_{x0}, \sigma_{y0}) T(\sigma_{x0}/\lambda, \sigma_{y0}/\lambda). \end{aligned} \quad (10)$$

Equation (10) is the well-known Fraunhofer diffraction formula<sup>4,5</sup> (except for the polarization factor  $\Psi_\alpha$ ). Note that this result is obtained directly from Eq. (6) by using the steepest-descent approximation without the need to go through the more complicated Kirchhoff theory.

The validity of the steepest-descent approximation is, in general, guaranteed if  $z_0$  is much larger than the linear di-

mensions of the initial distribution and if the observation point  $(x, y)$  is not far from the origin in the observation plane. For the purpose of comparing the Fraunhofer formula with the Fresnel patterns obtained in the next section, we rewrite Eq. (10) below, using dimensionless parameters  $x', y', z_0'$  to represent coordinates in units of wavelength:

$$\begin{aligned} t_\alpha(\lambda x', \lambda y', \lambda z_0') &= -i \frac{\exp(i2\pi z_0')}{z_0'} \\ &\quad \times \exp(i2\pi z_0' [1 + (x'^2 + y'^2)/z_0'^2]^{1/2} - 1]) \\ &\quad \times (1 - \sigma_{x0}^2 - \sigma_{y0}^2) \Psi_\alpha(\sigma_{x0}, \sigma_{y0}) \\ &\quad \times [\lambda^{-2} T(\sigma_{x0}/\lambda, \sigma_{y0}/\lambda)], \end{aligned} \quad (11a)$$

where

$$\lambda^{-2} T(\sigma_x/\lambda, \sigma_y/\lambda) = \begin{cases} \mathcal{F}\{t(\lambda x', \lambda y')\}, & \sigma_x^2 + \sigma_y^2 \leq 1, \\ 0, & \text{otherwise} \end{cases} \quad (11b)$$

Note that the second exponential term in Eq. (11a) is a curvature phase factor with radius of curvature  $z_0$ .

### 4. FRESNEL OR NEAR-FIELD DIFFRACTION

In general, Eq. (6) can be written as

$$\begin{aligned} t_\alpha(\lambda x', \lambda y', \lambda z_0') &= \exp(i2\pi z_0') \\ &\quad \times \mathcal{F}^{-1}\{\lambda^{-2} T(\sigma_x/\lambda, \sigma_y/\lambda) \Psi_\alpha(\sigma_x, \sigma_y)\} \\ &\quad \times \exp\{i2\pi z_0' [(1 - \sigma_x^2 - \sigma_y^2)^{1/2} - 1]\}, \end{aligned} \quad (12)$$

with  $T(\sigma_x/\lambda, \sigma_y/\lambda)$  given by Eq. (11b). This is the general statement of the Fresnel diffraction.

As an example, consider a circular aperture of radius  $R = 5\lambda$ , illuminated with a plane, linearly polarized beam propagating in the  $Z$  direction with polarization vector along the  $X$  axis. The Fresnel number  $N$  of this aperture as observed from a point on the optical axis at  $Z = z_0$  is given by<sup>6</sup>

$$z_0/\lambda = (1/N)(R/\lambda)^2 - (N/4). \quad (13)$$

At  $N = 1$  (corresponding to  $z_0 = 25\lambda$ ) the intensity distribution is as shown in Fig. 3. Figure 3(a) shows the intensity for the  $X$  component of polarization. The incident power on the aperture has been set to unity, and the calculated power for the distribution in Fig. 3(a) is 0.97; the peak intensity in this figure is  $I_{\max} = 0.05\lambda^{-2}$ . Figure 3b shows the intensity for the  $Z$  component of polarization; the power in this component is 0.01, and the peak intensity is  $0.18 \times 10^{-3} \lambda^{-2}$ . The  $Y$  component (not shown here) is an order of magnitude below the  $Z$  component, and its computation is somewhat complicated owing to the existence of truncation and round-off errors that are of the same order of magnitude as the signal itself. In any event, the polarization effects in this example are small and can safely be ignored. In the absence of the polarization factor  $\Psi_\alpha$ , the two-dimensional Fourier transforms in Eq. (12) can be reduced to one-dimensional Bessel transforms for circularly symmetric apertures. Figure 4 shows the radial distribution of intensity for the above aperture at  $z_0 = 12\lambda$  (corresponding to  $N = 2$ ) as computed with two successive Bessel transforms. The intensity here is normalized by the intensity at the aperture. Similar results can be obtained for other values of  $R$  and  $z_0$ , and all the well-

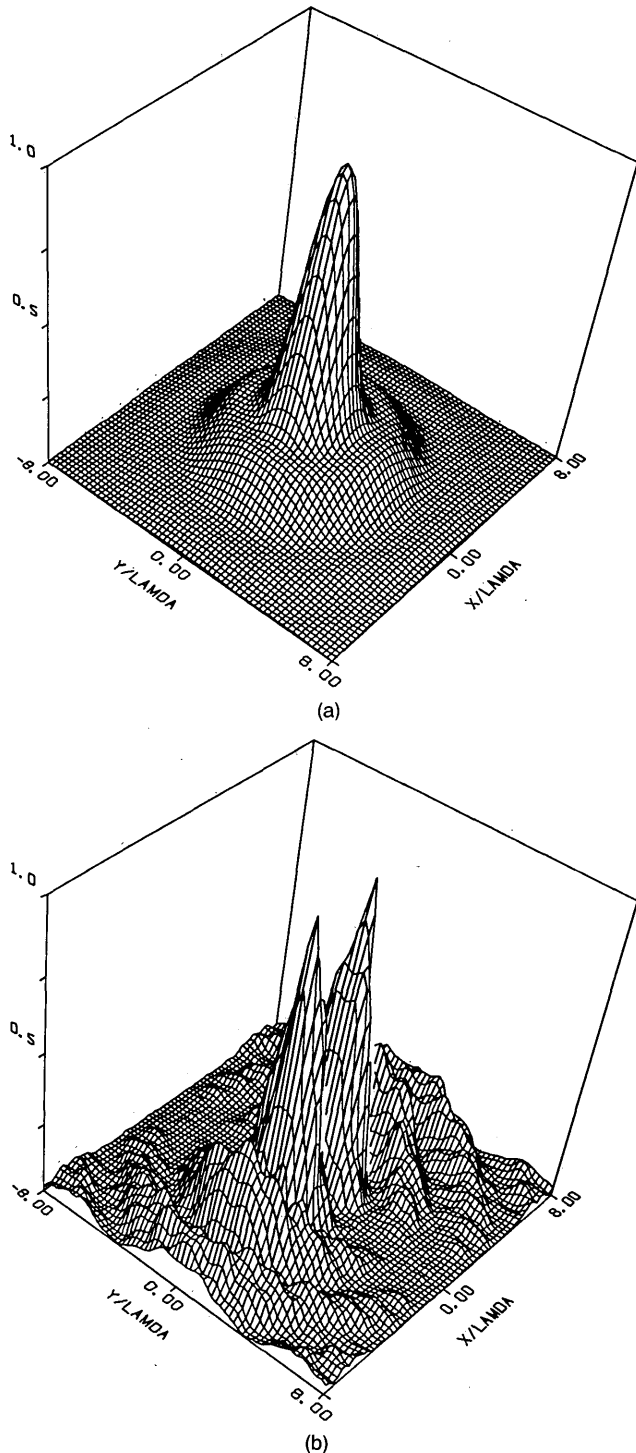


Fig. 3. Fresnel diffraction from a circular aperture of radius  $R = 5\lambda$  at a distance  $z_0 = 25\lambda$ . The X and Y axes are normalized by the wavelength  $\lambda$ , whereas the vertical axis has units of maximum intensity,  $I_{\max}$ . The incident beam is plane, propagating in the Z direction with unit incident power on the aperture. The incident polarization is linear in the X direction. (a) Intensity distribution for the X component of polarization,  $I_{\max} = 0.50 \times 10^{-1}$ . (b) Intensity distribution for the Z component of polarization,  $I_{\max} = 0.18 \times 10^{-3}$ .

known patterns of Fresnel diffraction can be computed from Eq. (12) by using two Fourier (or Bessel) transforms.

For values of  $N$  less than unity, computation of Eq. (12) becomes slow owing to the large number of oscillations of the

phase factor. Fortunately, this is the Fraunhofer regime, where the steepest-descent approximation is applicable. With reference to Eqs. (11), consider a circular aperture of radius  $R$ . The first dark ring in the Fraunhofer pattern of this aperture is at the angular position  $(\sigma_{x0}^2 + \sigma_{y0}^2)^{1/2} = 0.61/(R/\lambda)$ , independent of  $z_0$ . Ignoring the term  $N/4$  in Eq. (13) and approximating sine with tangent, we obtain for the radius of the first ring in the observation plane

$$r' = (x'^2 + y'^2)^{1/2} = 0.61 (R/\lambda)/N.$$

Notice that the Fresnel pattern with  $N = 1$  in Fig. 3(a) is already close to the Fraunhofer pattern with a hint of the first dark ring around  $r' = 0.61 \times 5 = 3$ . The steepest-descent approximation is usually acceptable for distances  $z_0$  corresponding to  $N \lesssim 1/2$ .

### 5. DIFFRACTION IN THE PRESENCE OF A LENS

A perfect (aberration-free) spherical lens converts an incident plane wave to a spherical wave converging toward the focal point. Ideally, therefore, a lens is a phase object with the following amplitude-transmission function:

$$t(x, y) = \tau_0(x, y) \exp[i(2\pi/\lambda)\{f - (f^2 + x^2 + y^2)^{1/2}\}]. \quad (14)$$

$\tau_0(x, y)$  includes the aperture function, possible aberrations, and the incident amplitude distribution. As before, the incident beam will be assumed to be linearly polarized in the X direction. If the polarization is not linear, its X and Y components should be treated separately and the final results superimposed.

When the oscillations of the complex exponential term in Eq. (14) are not prohibitive [i.e., when  $(f/\lambda)NA^2$  is relatively small], it is possible to treat Eq. (14) as an aperture function and use the Fresnel or Fraunhofer propagation formulas of the preceding sections. For example, in Farnell's experi-

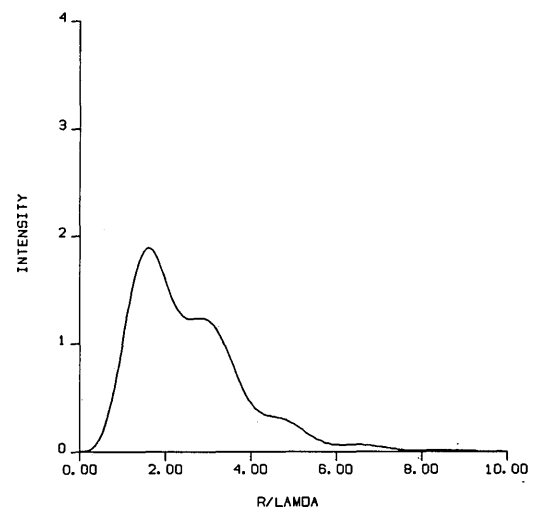


Fig. 4. Fresnel diffraction from a circular aperture of radius  $R = 5\lambda$  at a distance  $z_0 = 12\lambda$ . The incident beam is plane with unit intensity at the aperture. The polarization effects are ignored. The intensity at the observation plane has circular symmetry; thus only the radial distribution is shown. Notice that the central spot is dark and the peak intensity is twice the intensity of the incident beam at the aperture.

ments in the microwave-frequency range ( $\lambda = 3.22$  cm), the focal length and the numerical aperture were  $f = 20\lambda$  and  $NA = 0.36$ , respectively.<sup>7,8</sup> To compute the diffraction patterns for this case we used Eq. (12) in conjunction with Eq. (14) and set  $\tau_0(x, y) = 1$  in the aperture; the necessary array size was  $256 \times 256$ . We found that the maximum intensity on the optical axis occurs not at the focal point but at  $z_0 = 18\lambda$ , in agreement with Farnell's experimental findings. The computations also revealed that the maximum intensity is about 10% higher than the intensity at the focal point. As another example, we compared our results with theoretical results of Mahajan,<sup>9</sup> who calculated the axial intensity distribution for small numerical apertures. We used a  $128 \times$

Equation (18) is now used in the diffraction equation (12), yielding

$$t_\alpha(\lambda x', \lambda y', \lambda z_0') = -if' \exp(i2\pi z_0') \mathcal{F}^{-1} \{ \Psi_\alpha(\sigma_x, \sigma_y) \mathcal{F}\{h(u, v)\} \times \exp\{-i2\pi z_0' [1 - 1/2(f'/z_0')(\sigma_x^2 + \sigma_y^2) - (1 - \sigma_x^2 - \sigma_y^2)^{1/2}]\} \}. \quad (19)$$

Equation (19) can be written in the following compact form:

$$t_\alpha(\lambda x', \lambda y', \lambda z_0') = -if' \exp(i2\pi z_0') \mathcal{F}^{-1} \{ \Psi_\alpha(\sigma_x, \sigma_y) g(\sigma_x, \sigma_y) \}, \quad (20a)$$

where

$$g(\sigma_x, \sigma_y) = \begin{cases} \exp\left\{ i\pi \left[ (f' - z_0')(\sigma_x^2 + \sigma_y^2) - 2z_0' \sum_{n=2}^{\infty} \frac{(2n-3)!!}{2^n n!} (\sigma_x^2 + \sigma_y^2)^n \right] \right\} \mathcal{F}\{h(u, v)\} & \sigma_x^2 + \sigma_y^2 > 1 \\ 0, & \sigma_x^2 + \sigma_y^2 \leq 1 \end{cases} \quad (20b)$$

128 array for numerical computations corresponding to  $NA = 0.85 \times 10^{-4}$  and  $f = 139 \times 10^6 \lambda$  and reconstructed the curve in Fig. 7 of Mahajan's paper.

For large values of  $(f/\lambda)NA^2$ , the rapid oscillations of the lens-transmission function in Eq. (14) reduce the efficiency of computations to the extent that time and memory requirements make such computations impractical. Fortunately, however, it is possible to factor out the fast-oscillating term and apply the Fourier transformations to the remaining function. To show this, we rewrite Eq. (14) as follows:

$$t(\mathbf{f}\mathbf{x}, \mathbf{f}\mathbf{y}) = \tau(\mathbf{f}\mathbf{x}, \mathbf{f}\mathbf{y}) \exp[-i\pi f'(\mathbf{x}^2 + \mathbf{y}^2)]. \quad (15a)$$

Here  $\mathbf{x} = x/f, \mathbf{y} = y/f, f' = f/\lambda$ , and

$$\begin{aligned} \tau(\mathbf{f}\mathbf{x}, \mathbf{f}\mathbf{y}) &= \tau_0(\mathbf{f}\mathbf{x}, \mathbf{f}\mathbf{y}) \exp\{-i2\pi f'[(1 + \mathbf{x}^2 + \mathbf{y}^2)^{1/2} - 1 - 1/2(\mathbf{x}^2 + \mathbf{y}^2)]\} \\ &= \tau_0(\mathbf{f}\mathbf{x}, \mathbf{f}\mathbf{y}) \exp\left\{ i2\pi f' \sum_{n=2}^{\infty} (-1)^n \frac{(2n-3)!!}{2^n n!} (\mathbf{x}^2 + \mathbf{y}^2)^n \right\}. \end{aligned} \quad (15b)$$

Since  $t(\mathbf{f}\mathbf{x}, \mathbf{f}\mathbf{y})$  in Eq. (15a) is the product of two functions, its Fourier transform can be written as a convolution, namely,

$$\mathcal{F}\{t(\mathbf{f}\mathbf{x}, \mathbf{f}\mathbf{y})\} = \mathcal{F}\{\tau(\mathbf{f}\mathbf{x}, \mathbf{f}\mathbf{y})\} * (-i/f') \exp[i(\pi/f')(u^2 + v^2)], \quad (16)$$

where  $u$  and  $v$  are variables of the transform domain. Equation (16) can equivalently be written as

$$\begin{aligned} f^{-2} T(u/f, v/f) &= (-i/f') \exp[i(\pi/f')(u^2 + v^2)] \\ &\times \int \int_{-\infty}^{+\infty} h(u', v') \exp[-i(2\pi/f')(uu' + vv')] du' dv', \end{aligned} \quad (17a)$$

where, by definition,

$$h(u, v) = \exp[i(\pi/f')(u^2 + v^2)] \mathcal{F}\{\tau(\mathbf{f}\mathbf{x}, \mathbf{f}\mathbf{y})\}. \quad (17b)$$

Using dimensionless quantities  $\sigma_x = u/f'$  and  $\sigma_y = v/f'$ , Eq. (17a) becomes

$$\lambda^{-2} T(\sigma_x/\lambda, \sigma_y/\lambda) = -if' \exp[i\pi f'(\sigma_x^2 + \sigma_y^2)] \mathcal{F}\{h(u, v)\}. \quad (18)$$

The results can now be summarized as follows: To compute the diffraction pattern at  $Z = z_0$  follow these steps:

- (1) Calculate  $\tau(\mathbf{f}\mathbf{x}, \mathbf{f}\mathbf{y})$  according to Eq. (15b). [Note that  $\tau_0(\mathbf{f}\mathbf{x}, \mathbf{f}\mathbf{y}) = 0$  when  $(\mathbf{x}^2 + \mathbf{y}^2)^{1/2} > \tan[\arcsin(NA)]$ ].
- (2) Calculate  $h(u, v)$  from Eq. (17b).
- (3) Calculate  $g(\sigma_x, \sigma_y)$  from Eq. (20b).
- (4) Calculate  $t_\alpha(\lambda x', \lambda y', \lambda z_0')$  from Eq. (20a). (This step should be performed separately for the three components of polarization.)

We have thus shown that a sequence of three Fourier transforms yields the diffraction pattern around the focal plane of a lens. It is instructive to derive the standard single-Fourier-transform lens formula from these results. In the limit when  $NA \lesssim 4\sqrt{\lambda}/f$ , the infinite sums in Eqs. (15b) and (20b) are close to zero and can be ignored. Thus  $\tau(x, y) = \tau_0(x, y)$  and  $g(\sigma_x, \sigma_y) = \mathcal{F}\{h(u, v)\}$  at  $z_0 = f$ . If polarization effects are ignored, Eq. (20a) would yield

$$\begin{aligned} t(\lambda x', \lambda y', \lambda f') &= -if' \exp(i2\pi f') \mathcal{F}^{-1}\{\mathcal{F}\{h(u, v)\}\} \\ &= -(f/\lambda) \exp(i2\pi f/\lambda) \exp[i(\pi\lambda/f)] \\ &\times (x'^2 + y'^2) \mathcal{F}\{\tau_0(\mathbf{f}\mathbf{x}, \mathbf{f}\mathbf{y})\}. \end{aligned} \quad (21)$$

Equation (21) is the well-known result of diffraction theory that is usually obtained from the Fresnel-Kirchhoff integral under standard approximations.<sup>4</sup>

## 5. RESULTS AND DISCUSSION

In this section we present results of numerical computations for a lens with  $f = 4000\lambda$  and  $NA = 0.3$ . Figure 5(a) shows the function  $\tau(x, y)$  versus distance from the lens center (only the real part of the function is shown); it has been assumed that  $\tau_0(x, y) = 1$  within the aperture. The oscillations are due to the complex exponential function in Eq. (15b). After two Fourier transformations and multiplications by various phase factors in the process, the function  $g(\sigma_x, \sigma_y)$  is obtained whose real and imaginary parts at  $z_0 = f$  are plotted in Fig. 5(b) versus  $(\sigma_x^2 + \sigma_y^2)^{1/2}$ . Here, as in Fig.

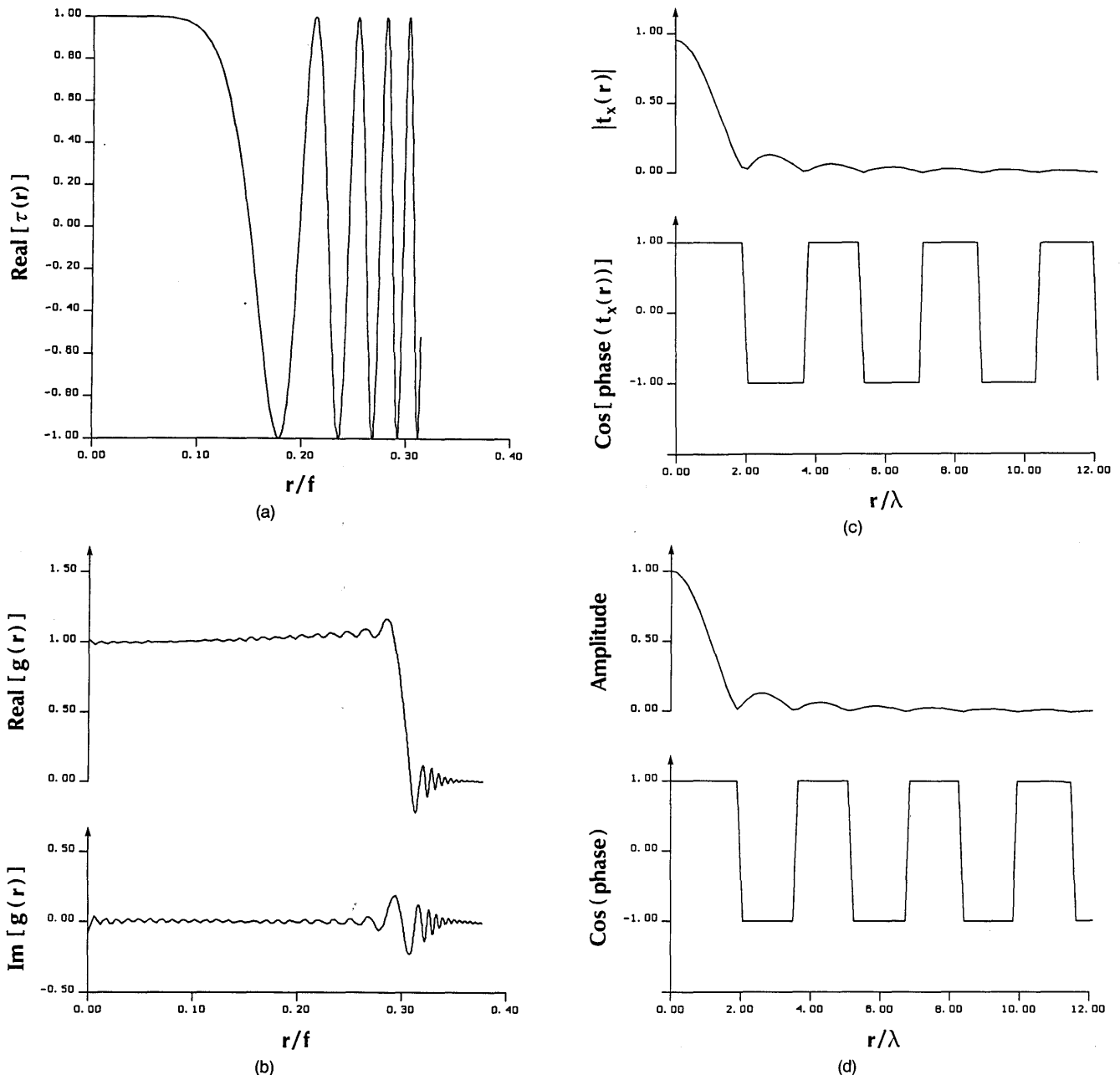


Fig. 5. Diffraction from aberration-free, spherical lens with  $f = 4000\lambda$  and  $NA = 0.3$ . The incident beam is plane with unit amplitude, and the polarization effects are ignored. (a) The real part of the complex function  $\tau(x, y)$  versus the normalized distance from the lens center. (b) The real and imaginary parts of the complex function  $g(\sigma_x, \sigma_y)$  versus  $(\sigma_x^2 + \sigma_y^2)^{1/2}$  at  $z_0 = f$ . (c) Amplitude and phase of the distribution at the focal plane. The amplitude is normalized by the aperture area of the lens. (d) Amplitude and phase of the distribution at the focal plane obtained with standard approximations.

5(a), the horizontal axis can be interpreted as the normalized distance from the lens center. Finally, a third Fourier transform as described by Eq. (20a) yields the distribution at the focal plane. We have ignored the polarization effects at this stage by setting  $\Psi_\alpha = 1$  and computed  $t(\lambda x', \lambda y', \lambda f')$ , which is then plotted versus radial distance from the focal point as shown in Fig. 5(c). Both amplitude and phase of the distribution are shown here, and the amplitude is normalized by the aperture area of the lens. To compare this result with the standard approximate distribution, otherwise known as the Airy pattern, we have plotted the corresponding function, as described by Eq. (21), in Fig. 5(d). Notice that the

peak amplitude in Fig. 5(c) is slightly less than that of Fig. 5(d) and that the zeros of the exact distribution are slightly shifted to the right of the corresponding zeros of the Airy pattern. These differences are expected to be more pronounced at larger numerical apertures.

The effects of polarization are shown in the two-dimensional plots of intensity at the focal plane in Fig. 6; a plane incident beam has been assumed with unit power in the aperture and linear polarization in the X direction. Figure 6(a) corresponds to the X component of polarization in the focal plane; the total power in this component is 0.976, and the peak intensity is  $0.276\lambda^{-2}$ . Figure 6(b) shows the inten-

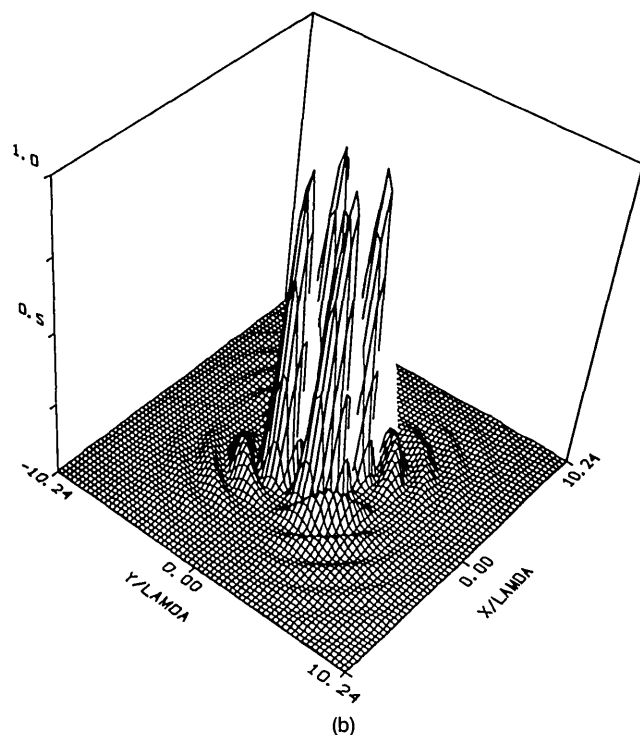
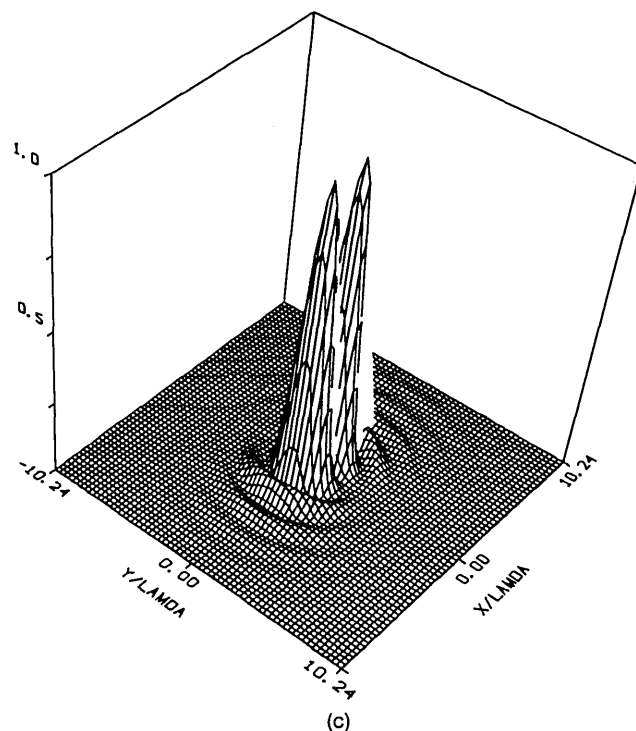
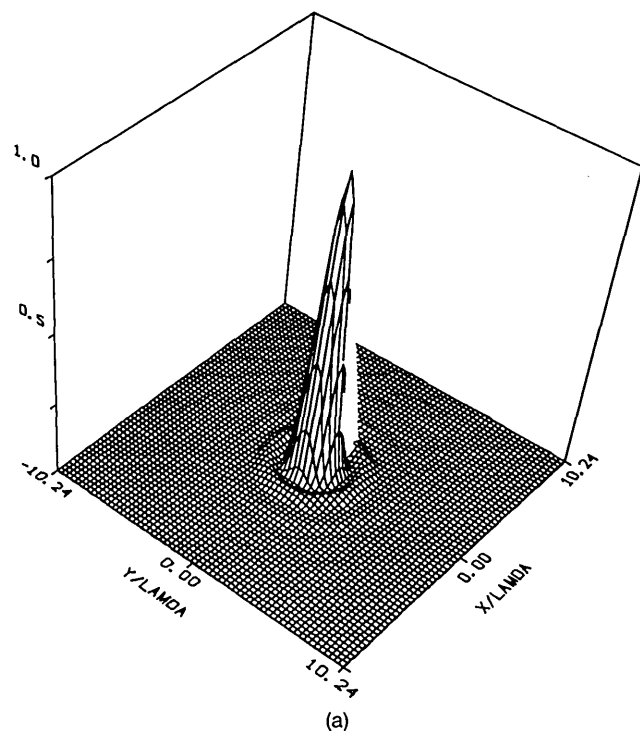


Fig. 6. Diffraction from aberration-free, spherical lens with  $f = 4000\lambda$  and  $NA = 0.3$ . The incident beam is plane, is linearly polarized in the  $X$  direction, and has unit power in the aperture. (a) Intensity distribution for the  $X$  component of polarization at the focal plane.  $I_{\max} = 0.276\lambda^{-2}$ . (b) Intensity distribution for the  $Y$  component of polarization in the focal plane.  $I_{\max} = 0.740 \times 10^{-5} \lambda^{-2}$ . (c) Intensity distribution for the  $Z$  component of polarization in the focal plane.  $I_{\max} = 0.335 \times 10^{-2} \lambda^{-2}$ .

sity distribution for the  $Y$  component of polarization with a total power of  $0.92 \times 10^{-4}$  and a peak intensity of  $0.74 \times 10^{-5} \lambda^{-2}$ . Figure 6(c) corresponds to the  $Z$  component of polarization with a total power of 0.023 and a peak intensity of  $0.335 \times 10^{-2} \lambda^{-2}$ . Notice that the  $Y$  component has four peaks located in the four quadrants of the  $XY$  plane, while the  $Z$  component has only two peaks, which are separated in the direction of the incident polarization.

Finally, the intensity distribution at  $z_0 = f + 15\lambda$  is shown in Fig. 7. (Only the  $X$  component of polarization is shown.) The total power in this component is again 0.976, but the peak intensity is only  $0.04\lambda^{-2}$ . The same distribution was found for  $z_0 = f - 15\lambda$ . Note that the depth of focus ( $\lambda/NA^2$ ) for the lens studied here is about  $10\lambda$ .

For the computations leading to Figs. 6 and 7 we used a  $512 \times 512$  array and a standard two-dimensional fast-Fouri-

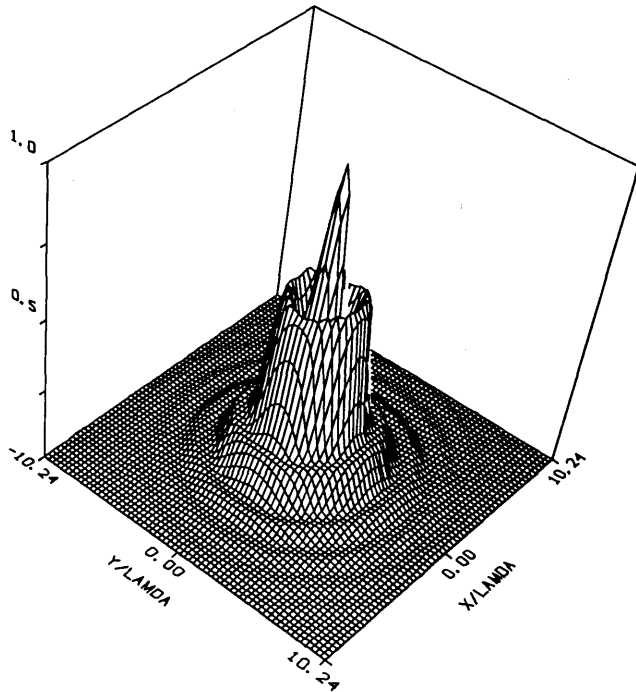


Fig. 7. Intensity distribution for the X component of polarization at  $z_0 = f \pm 15\lambda$  (same lens as Fig. 6).  $I_{\max} = 0.4 \times 10^{-1} \lambda^{-2}$ .

er-transform algorithm; on a VAX11/780 computer, the entire process took less than 10 min. For larger numerical apertures and/or focal lengths the array size increases [the linear dimensions of the array are proportional to the focal length and to the fourth power of  $\tan[\arcsin(\text{NA})]$ ], but the computational requirements remain within the reach of present-day computers.

## REFERENCES

1. H. H. Hopkins, "The Airy disk formula for systems of high relative aperture," *Proc. Phys. Soc. London* **55**, 116-128 (1943).
2. M. Born and E. Wolf, *Principles of Optics*, 6th ed. (Pergamon, Oxford, 1980).
3. J. D. Jackson, *Classical Electrodynamics*, 2nd ed. (Wiley, New York, 1975).
4. J. W. Goodman, *Introduction to Fourier Optics* (McGraw-Hill, New York, 1968).
5. M. V. Klein, *Optics* (Wiley, New York, 1970).
6. F. Jenkins and H. White, *Fundamentals of Physical Optics*, 1st ed. (McGraw-Hill, New York, 1937).
7. G. W. Farnell, "Measured phase distribution in the image space of a microwave lens," *Can. J. Phys.* **36**, 935-943 (1958).
8. Y. Li and E. Wolf, "Three-dimensional intensity distribution near the focus in systems of different Fresnel numbers," *J. Opt. Soc. Am. A* **1**, 801-808 (1984).
9. V. N. Mahajan, "Axial irradiance and optimum focusing of laser beams," *Appl. Opt.* **22**, 3042-3053 (1983).